Control of Horizontal Convection Forcing Boundary Layer Instability Using a Tuned ZNMF Oscillating Jet

M.A. Leigh[1], T.K. Tsai[1] and G.J. Sheard[1]

[1]Department of Mechanical and Aerospace Engineering
Monash University, Clayton, Victoria 3800, Australia

Abstract

Horizontal convection driven by a linear temperature profile along the bottom of a two dimensional rectangular enclosure is perturbed by a small tuned zero-net-mass-flux (ZNMF) jet. At a Rayleigh number below the natural onset of instability, the boundary layer is found to be convectively unstable, exhibiting a disturbance pattern consistent with a Rayleigh-Bénard mechanism. Nusselt number is enhanced across a range of frequencies for all perturbation amplitudes, with the response dominated by two frequencies differing by approximately a factor of two: each invokes the shedding of pulsing vortices moving through the vertical end-wall plume at the higher frequency. This points to a natural sensitivity in this flow to disturbances convecting in the upstream boundary layer.

Introduction

Horizontal convection is a form of convection in which the flow is triggered by a heating differential applied across one horizontal boundary, either at the top or bottom boundary. Unlike the comprehensively studied Rayleigh-Bénard convection, in which vertical heating from below promotes overturning, in horizontal convection the heating on the uneven forcing boundary leads to overturning of the fluid [3]. Horizontal temperature gradients are found in geophysical flows, including the Earth's oceans, atmosphere and mantle [1].

The characteristics of horizontal convection are highly dependent on the Rayleigh number, which indicates the strength of the heating differential. Fluid flow at low Rayleigh numbers is laminar and diffusive in nature; no boundary layer is present. Overturning circulation is approximately symmetrical and is caused by the destabilizing buoyancy input. At higher Rayleigh numbers the fluid flow moves from diffusion-dominated to convection-dominated and a thermal and velocity boundary layer begin to form along the horizontal boundary where the differential temperature is applied [9].

Above a critical Rayleigh number the flow becomes unsteady. Instability presents as mushroom shaped plumes breaking out from the boundary layer and eddies forming within the vertical plume, which transports the hotter, more buoyant fluid towards the top of the tank before it recirculates horizontally along the top and diffuses in the interior of the box. Understanding the nature of the instabilities in horizontal convection is important as controversy remains regarding both the transition to unstable flow and the role of turbulence in the flow. Earlier research suggested that horizontal convection is not turbulent [8], however recent experimental and numerical studies have indicated horizontal convection does feature instabilities and turbulence [7,9,2].

While the manifestation of instability in horizontal convection is increasingly well understood [2,3,9], the characteristics of the underlying instability mechanism is less clear. Working on the hypothesis that instability originates within the forcing boundary
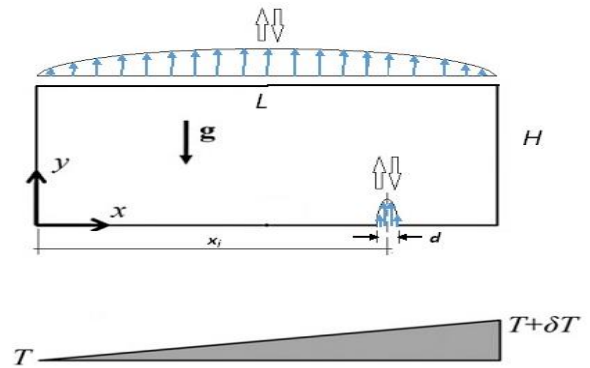

Figure 1. Schematic representation of the two-dimensional problem under consideration.

layer, the present study seeks to investigate the response of a horizontal convection flow a little below the onset of unsteady flow to a controlled, localized perturbation. The perturbation is implemented using a periodic oscillation of a small ZNMF jet embedded flush with the forcing boundary.

Numerical Model and Methodology

Model Description

Figure 1 shows a schematic of the problem being investigated – a two dimensional fluid undergoing horizontal convection in a rectangular box with height, H, and width, L, where consistent with Mullarney et al. [7], a fixed $H/L = 0.16$ is used. The flow is instigated by applying a linear temperature profile on the base of the enclosure. The remaining three walls are perfectly insulated. The two side walls have a no slip boundary condition. The bottom surface has a no slip boundary condition with the exception of the ZNMF jet location, while the upper horizontal boundary has a second broad and weak ZNMF jet to satisfy conservation of mass. There are numerous parameters involved in quantifying the periodic perturbation – these include the ZNMF jet amplitude, A, frequency, ω, position, x_j and orifice width, d.

This work seeks to characterise the response of the flow via the Nusselt number to boundary-layer perturbation of specific amplitude and frequency.

Governing Equations

The governing equations are the dimensionless Navier-Stokes equations for a Boussinesq fluid, which are expressed as

$$\frac{\partial \boldsymbol{u}}{\partial t} = -(\boldsymbol{u} \cdot \nabla)\boldsymbol{u} - \nabla p + Pr\nabla^2\boldsymbol{u} - PrRa\hat{\boldsymbol{g}}T, \qquad (1)$$

$$\nabla \cdot \boldsymbol{u} = 0, \qquad (2)$$

$$\frac{\partial T}{\partial t} = -(\boldsymbol{u} \cdot \nabla)T + \nabla^2 T, \qquad (3)$$

where $\boldsymbol{u}$, t, p, Pr, Ra, $\boldsymbol{\hat{g}}$ and T are the velocity vector, time, static pressure (kinematic), Prandtl number, Rayleigh number, gravity unit vector and temperature of the fluid respectively. In this study lengths, velocities, time, pressure and temperature are scaled by L, κ_T/L, L^2/κ_T, $\rho_0\kappa_T{}^2/L^2$ and δT respectively. κ_T is the thermal diffusivity of the fluid, ρ_0 is a reference density and δT is the temperature difference applied along the bottom boundary.

The Rayleigh number is defined as

$$Ra = \frac{g\alpha\delta T L^3}{\nu K_T}, \qquad (4)$$

where g is the acceleration due to gravity , α is the thermal expansion coefficient and ν is the kinematic viscosity of the fluid.

The Prandtl number is defined as

$$Pr = \frac{\nu}{K_T}. \qquad (5)$$

A Prandtl number of 6.14 is used for this study, which is consistent with water at room temperature.

The Nusselt number, which is the ratio of convective to conductive heat transfer, is defined as

$$Nu = \frac{F_T L}{\rho_0 c_p K_T \delta T}, \qquad (6)$$

where F_T is the time average of the absolute heat flux along the forcing boundary and c_p is the specific heat capacity of the fluid.

The velocity profile for the ZNMF jet applied at the forcing boundary is parabolic with position and sinusoidal with time and is defined as

$$v_j = \left[1 - \frac{4}{d^2}(x - x_j)^2\right] v_1 \sin(\omega t), \qquad (7)$$

where v_1 is the maximum velocity of the ZNMF jet. The velocity, v_j, is valid over $x_j - d/2 \leq x \leq x_j + d/2$, $t \geq 0$.

A jet position of $x_j = 0.75L$ and width of $d = 0.1$ was used for the entirety of the analysis with the intention of positioning the jet where instabilities are first identified in the non-perturbed case and selecting a width such that the ZNMF jet would not significantly disrupt the boundary layer.

Previous studies of a similar numerical model identified instabilities within the flow occurring at Rayleigh numbers beyond 10^9 [9]. A Rayleigh number of 2.5×10^8 is used for this study, which is below the critical Rayleigh number but sufficiently high to enable instabilities initiated by the ZNMF jet to propagate downstream.

Jet amplitudes up to $v_1 = 1000$ are considered in this study, which corresponds to the maximum jet flow rate being approximately two-thirds of the horizontal flow in the kinematic boundary layer at that point. Hence the jet flows are always less than the unperturbed boundary layer flow and can therefore be regarded as a perturbation of, rather than an obliteration of, the boundary layer.

Numerical Method

The governing equations are solved numerically using a high-order solver implementing a spectral element method for spatial discretisation and a third-order time integration scheme for the two dimensional rectangular enclosure with the aforementioned applied perturbation. The solver has been validated and employed for horizontal convection flows, including in Sheard and King [9] and Hussam et al. [4]. The spectral element method combines the desirable convergence properties of the spectral
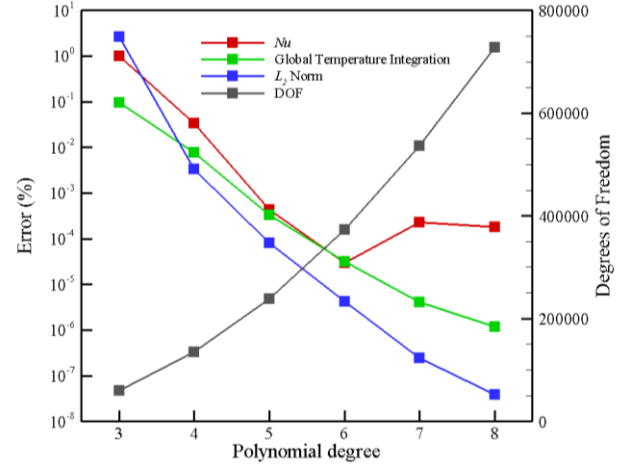

Figure 2. Percentage error for the global temperature integration, L_2 norm and the Nusselt number at the lower boundary against polynomial degree. The degrees of freedom (DOF) for each polynomial degree is also shown.

method and the geometric flexibility of the finite element method [5].

A mesh consisting of 3692 rectangular elements with a coarser mesh in the centre of the domain and a greater number of elements in close proximity to the boundaries to resolve the flow was used.

Three parameters were monitored in a grid resolution study – the integration of the temperature over the whole domain, the L_2 norm of the flow and the Nusselt number at the lower boundary. The results for varying polynomial degree are shown in figure 2. The percentage error is defined as the difference between the parameter value at the current element polynomial degree and the previous polynomial degree divided by the parameter value at the previous polynomial degree. The percentage error approximately decreases exponentially as the order of the shape function increases, which is a desirable property of the spectral element method [6]. An element polynomial degree of six is used henceforth, resulting in a total of 132,912 nodes (36 nodes per element) and 372,564 degrees of freedom.

Results and Discussion

Figure 3 plots the Nusselt number at the lower boundary of the enclosure against the frequency of the ZNMF jet for a variety of amplitudes of the ZNMF jet. The baseline case (no perturbation) is shown on the plot as a horizontal dashed line. Each curve displays a substantial increase in the Nusselt number initially over a large range of frequencies ($0 < \omega \lesssim 10^4$). As the perturbation frequency continues to increase, the elevated levels of heat transfer decrease until the Nusselt number approaches the baseline case at larger frequencies.

Two distinct peaks are evident in the Nusselt number within the excited frequency range. Firstly, a frequency of $\omega \approx 4000$ results in a spike in the Nusselt number at higher amplitudes ($A \gtrsim 10$).

This lower frequency mode is likely to be associated with a forced convection arrangement. Secondly, at lower amplitudes ($A \lesssim 100$) a perturbation frequency of approximately 7500 results in a strong peak in the Nusselt number, indicating a natural convection regime.

The appearance of two distinct local maxima at different frequencies is strongly suggestive of two unique modes of response being excited by the applied perturbation. To explore this further, the dependence of each of these peaks on
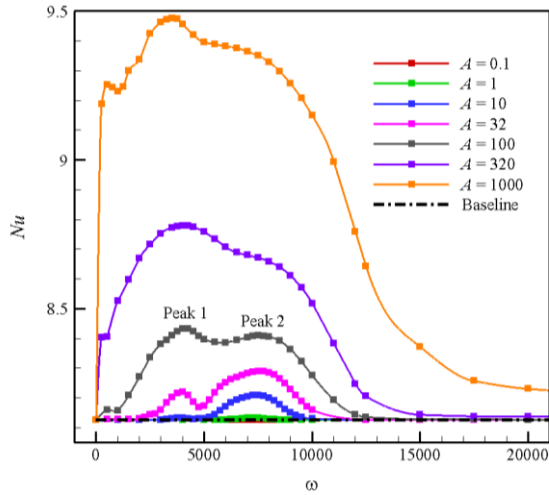
Figure 3. Nusselt number at the lower boundary against the frequency of the ZNMF jet. Akima splines have been fitted to the data.

perturbation amplitude is analysed and subsequently visualisation of the disturbed flows is included.

The peak Nusselt number against amplitude is shown in figure 4, which reveals the scaling of heat transfer with perturbation amplitude. The peak Nusselt number changes from the forced convection peak to the natural convection peak at a crossover amplitude of approximately $A_c \approx 75$. It is found that the Nusselt number increase over the baseline case ($\Delta Nu = Nu - Nu_0$, where Nu_0 is the Nusselt number of the baseline case) scales with amplitude through $\Delta Nu \sim A^{3/5}$ at higher amplitudes. For varying perturbation amplitude, Peak 1 consistently occurs at a frequency of approximately 4000, while Peak 2 is observed at a frequency of approximately 7500.

Figures 5 shows a snapshot of the temperature field for a perturbation amplitude of 32 and frequency of 4000. The effects of the perturbation are evident in the oscillating boundary layer downstream of the ZNMF jet (located at $x = 0.7L$). As the amplitude is increased the effect on the boundary layer becomes more pronounced. Peak 1, which occurs at a lower frequency, shows an unsteady circulation forming beyond the perturbation, which continues to propagate downstream until the end wall is reached. The end wall plume transfers the destabilizing buoyancy to the top of the enclosure before it diffuses into the centre of the enclosure. As the perturbation frequency is increased to the frequency which correlates with Peak 2, the spatial horizontal wavelength of the disturbance wave along the boundary layer decreases.

The fast Fourier transform (FFT) of the L_2 norm time history for the two dominant modes at frequencies 4000 and 7500 and an amplitude of 32 are shown in figure 6. The first harmonic occurs at the perturbation frequency for each case and subsequent harmonics occur at multiples of the perturbation frequency (ω, 2ω, ..., $n\omega$). Significantly more harmonics are seen in Peak 1 ($n = 11$) than Peak 2 ($n = 6$). The second harmonic of Peak 1 is similar in magnitude to the first harmonic, while the harmonics of the Peak 2 case decay monotonically with increasing frequency. This second harmonic for Peak 1 reveals a strong response in the flow that corresponds to a frequency that is approximately the same as the perturbation frequency for Peak 2. The Peak 1 case is being perturbed at approximately half the frequency of the Peak 2 case, but ultimately the end-wall plume emits vortices at a similar frequency to the Peak 2 mode. This suggests that these two perturbation frequencies are exciting a natural frequency of the end wall plume at this Rayleigh number. This is shown in figure 4 (b), where the frequency of the second
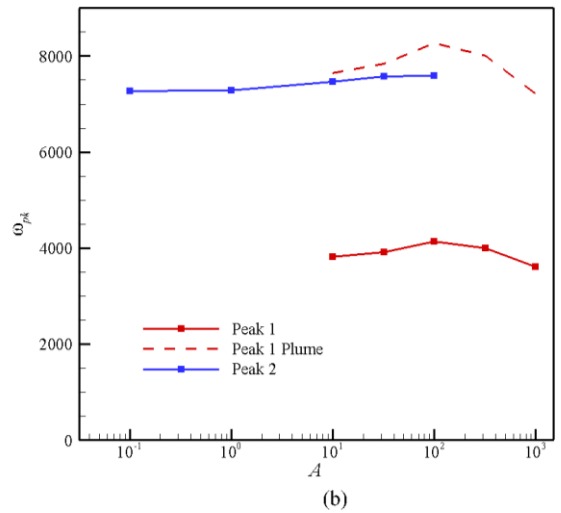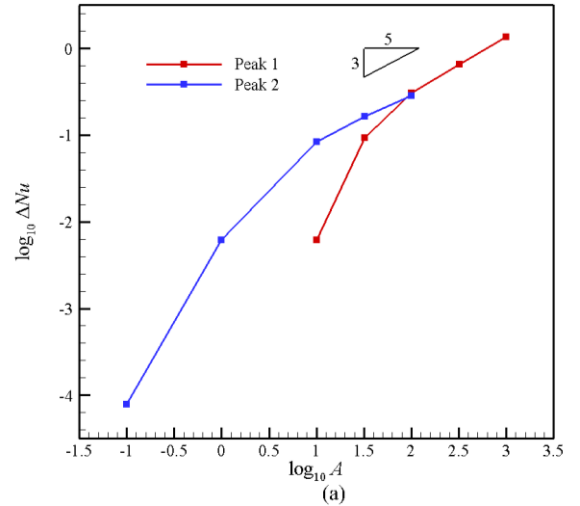

(a)

(b)

Figure 4. Delta peak Nusselt number at the lower boundary (log) against the amplitude of the ZNMF jet (log) (a) and peak perturbation frequency against the perturbation amplitude (b).

Figure 5. Temperature field snapshot for a perturbation amplitude of 32 and frequency of 4000 (Peak 1). Cooler regions are black, hotter regions are white.

harmonic for Peak 1 is similar in magnitude to the frequency of the Peak 2 perturbation.

By subtracting the vorticity field of the baseline case from the vorticity field found with the ZNMF jet present, the disturbance vorticity field is produced, as is shown in figures 7 and 8 for a perturbation amplitude of 32 and frequencies of 4000 (Peak 1) and 7500 (Peak 2), respectively. Both cases show similarities to Rayleigh-Bénard convection instability as evidenced by paired positive and negative vortices within the forcing boundary layer that grow in strength as they move towards the end wall. There they seed the ejection of eddies vertically upward into the end-wall plume. Considering the Peak 1 case, the strong positive vorticity region (indicated in red) in the lower right hand corner is transported up the right hand wall to the top of the enclosure before it is ejected towards the centre of the domain. Meanwhile, at approximately half the perturbation period, a second strong positive vortex begins to form, which follows the same sequence and is ejected from the end wall plume. In contrast, Peak 2 transports one strong positive vortex through the end wall plume over the oscillation period. This demonstrates that the plume is
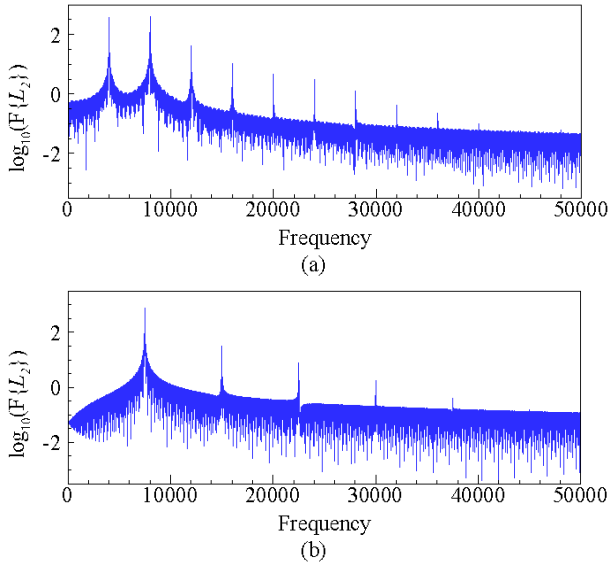
Figure 6. FFT of the L_2 norm for a perturbation amplitude of 32 and frequency of (a) 4000 (peak 1) and (b) 7500 (peak 2).
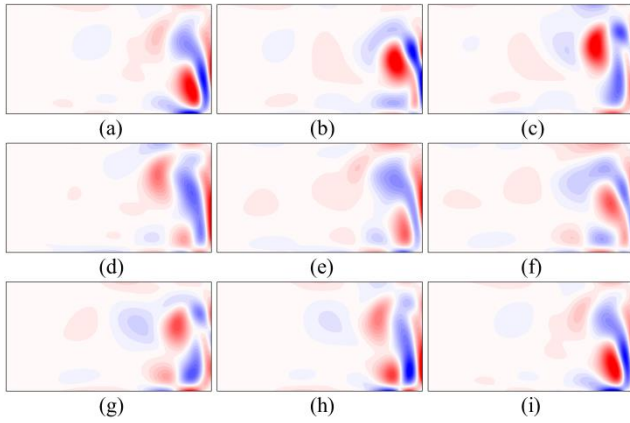

Figure 7. Time sequence of the disturbance vorticity field for a perturbation amplitude of 32 and frequency of 4000 (Peak 1). The area shown is the full height of the enclosure and $0.7L \leq x \leq L$. Red indicates strong positive vorticity, blue is negative vorticity and white is zero vorticity. The sequence is one perturbation period in length.

shedding at the first harmonic frequency (8000) for Peak 1, and at the driving frequency (7500) for Peak 2. This is reflected in the FFT spectra in figure 6, which shows Peak 1 has approximately twice as many distinct harmonics. The jet disturbance is similar for both modes, suggesting that the different driving frequencies excite the same natural instability mechanism in the plume.

Conclusions

Numerical simulations of horizontal convection driven by a linear temperature profile along the bottom of a two dimensional rectangular enclosure with an applied periodic perturbation have been carried out. These simulations demonstrate that a substantial increase in the Nusselt number over the non-perturbed case is exhibited over a large range of applied perturbation frequencies ($0 < \omega \lesssim 10^4$). Two distinct peaks of Nusselt number occur, suggesting a forced convection and natural convection mode. Instabilities are evident in the forcing boundary layer that lead to ejection of eddies in the end wall plume and vortex pairs forming, similar to Rayleigh-Bénard convection instability. Despite being driven by two perturbation frequencies that differ by a factor of approximately two, ultimately both of these resultant modes are a consequence of
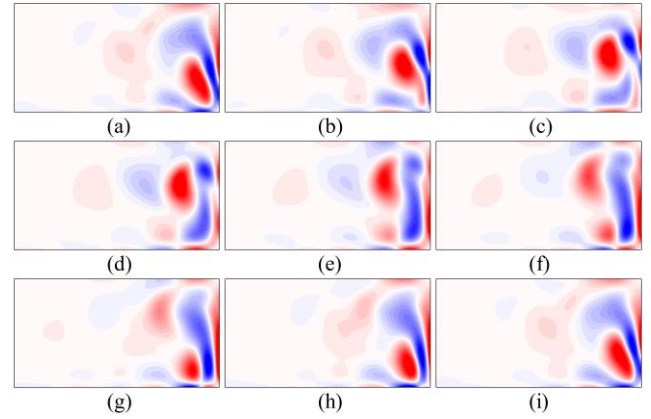

Figure 8. Time sequence of the disturbance vorticity field for a perturbation amplitude of 32 and frequency of 7500 (Peak 2). The area shown is the full height of the enclosure and $0.7L \leq x \leq L$. Red indicates strong positive vorticity, blue is negative vorticity and white is zero vorticity. The sequence is one perturbation period in length.

exciting the same natural frequency in the plume, which is approximately 7500.

Acknowledgments

References

[1] Beardsley, R.C. & Festa J.F., A Numerical Model of Convection Driven by a Surface Stress and Non-uniform Horizontal Heating, *Journal of Physical Oceanography*, **2**, 1972, 444-455.

[2] Gayen, B., Griffiths, R.W. & Hughes, G.O., Stability Transitions and Turbulence in Horizontal Convection, *Journal of Fluid Mechanics*, **751**, 2014, 698-724.

[3] Hughes, G.O. & Griffiths, R.W., Horizontal Convection, *Annual Review of Fluid Mechanics,* **40**, 2008, 185-208.

[4] Hussam, W.K., Tsai, T.K. & Sheard, G.J., The Effect of Rotation on Radial Horizontal Convection and Nusselt Number Scaling in a Cylindrical Container, *International Journal of Heat and Mass Transfer*, **77**, 2014, 46-59.

[5] Karniadakis, G.E., Israeli, M. & Orszag, S.A., High-order Splitting Methods for the Incompressible Navier-Stokes Equations, *Journal of Computations Physics*, **97**, 1991, 414-443.

[6] Karniadakis, G.E. & Sherwin, S.J., *Spectral/hp Element Methods for Computational Fluid Dynamics*, Oxford University Press, 2005.

[7] Mullarney, J.C., Griffiths, R.W. & Hughes, G.O., Convection Driven by Differential Heating at a Horizontal Boundary, *Journal of Fluid Mechanics*, **516**, 2004, 181-209.

[8] Paparella, F. & Young, W.R., Horizontal Convection is Non-turbulent, *Journal of Fluid Mechanics*, **466**, 2002, 205-214.

[9] Sheard, G.J. & King, M.P., Horizontal Convection: Effect of Aspect Ratio on Rayleigh Number Scaling and Stability, *Applied Mathematical Modelling,* **35**, 2011, 1647-1655.